Early Stage Interplay of Microphase Separation and Crystallization in Crystalline−Coil Poly(L-lactic acid)-*block*-polystyrene Thin Films

Jun Fu,[†,§] Bin Luan,[‡] Caiyuan Pan,[‡] Binyao Li,[†] and Yanchun Han*,[†]

State Key Laboratory of Polymer Physics and Chemistry, Changchun Institute of Applied Chemistry, Graduate School of the Chinese Academy of Sciences, Chinese Academy of Sciences, 5625 Renmin Street, Changchun 130022, P. R. China, and Department of Material Science and Engineering, University of Science & Technology of China, Hefei 230026, P. R. China

Received August 16, 2004; Revised Manuscript Received April 25, 2005

ABSTRACT: The interplay of microphase separation and crystallization has been investigated at the early stage of annealing the amorphous thin films of the crystalline−coil poly(L-lactic acid)-*block*-polystyrene (PLLA-*b*-PS) diblock copolymer. The homogeneous and heterogeneous films were annealed at the temperatures between the glass transition temperature of PS (T_g^{PS}) and the melting point of PLLA (T_m^{PLLA}) so that the microphase separation and crystallization were simultaneously possible. (1) The homogeneous films formed spinodal-like pattern, with the amplitude amplified to the lamellar spacing (L_0), indicating the microphase separation and perpendicular orientation of the copolymer chains with respect to the surface and substrate. Afterward, abnormal relief structures (domain II, ∼30 nm in height) started and grew laterally within the original relief patterns (domain I). The surface wavevector q decayed with the time t as $q \sim t^{-1/3}$, while the growth of domain II could be described by the Avrami equation with the exponent of 1.0. It was hypothesized that the PLLA may crystallize within the mesophase, increasing the lamellar spacing. (2) Using THF/CS_2 mixtures as solvent, semicrystalline nuclei were integrated to the spin-coated PLLA-*b*-PS films. These nuclei initiated the crystallization of the thin films. The crystallization kinetics follows the Avrami equation with the exponent of 2.6. The crystallization induced cracks in the films, which nucleated holes at the surface. The coarsening kinetics of the holes is an Ostwald ripening type. Comparison of the crystallization halftimes of the homogeneous and heterogeneous films suggests that the crystallization of these films may be a relaxation-controlled process.

1. Introduction

Diblock copolymers in strong segregation limit can spontaneously form ordered structures from melt due to the repulsive interaction between the unlike blocks.[1,2] Such highly ordered mesophase has been demonstrated to strongly influence the behavior of individual block chain, such as diffusion,[3] folding,[4−9] and so on. In particular, highly ordered segregated structures of block copolymers provide well-defined model for investigation of polymer crystallization within confined geometry.

Crystallization within the mesophases including spheres, cylinders, and lamellae has attracted increasing interest because of the involvement of hierarchical ordering and the complex interplay between the mesophase and the chain folding and unfolding.[4−9] When the segregation strength is sufficiently high, the crystallization is strictly confined in the cylinders or spheres even though the matrices were rubbery.[8,9] Such soft confinement has been proved to favor orientation of crystal stems perpendicular to the cylinder axis or the lamella plane.[6,9,11] First-order crystallization kinetics within strictly confined geometry have been reported,[8−13] in contrast to the bulk behavior with Avrami exponent $n = 2.0−4.0$, and was suggested to originate from the homogeneous nucleation process. By far, however, although the late stage interplay between the crystallization and microphase separation has obtained quite penetration, less is known about how these two ordering processes interact each other once the copolymer chains are able to relax above the glass transition temperature (T_g).

In this paper, we focus on the early stage interplay between the microphase separation (MPS) and crystallization. At temperatures above T_g but below melting point (T_m), the copolymer chains begin to relax so that MPS and crystallization are simultaneously possible. The competition and interplay between MPS and crystallization, therefore, may be expected. In thin films, the preferential attraction from the surface and substrate may usually induce orientation and stretching of copolymer chains,[14] which has been argued to be able to homogeneously nucleate crystallization in segregated phase.[11,12,15] On the other hand, polymer crystallization can be nucleated homogeneously or heterogeneously. Heterogeneous nucleation by nuclei is usually much faster than the homogeneous nucleated process since the thermal nucleation from the homogeneous overcooled polymeric liquid is very slow.

2. Experiments

2.1. Materials. The diblock copolymer, poly(L-lactic acid)-*block*-polystyrene (PLLA-*b*-PS) was synthesized by sequential atom transfer radical polymerization (ATRP) of styrene monomers and ring-opening polymerization (ROP) of L-lactide.[16] The number-average molecular weight is 19 800 (9400-*b*-10400) (total degree of polymerization $N = 230$) by ^{1}H NMR, and the polydispersity is less than 1.2 by gel permeation chromatography (GPC). Thus, the copolymer is approximately symmetric with 0.42 (volume fraction) PLLA and 0.58 PS blocks. The glass transition temperatures (T_g's) by differential scanning calorimeter (DSC) are 90 °C for PS and 55 °C for PLLA blocks.[17] The PLLA crystals have a peak melting point (T_m)

† Chinese Academy of Sciences.
‡ University of Science & Technology of China.
§ Present address: Max Planck Institute for Polymer Research, Ackermannweg 10, 55128 Mainz, Germany. E-mail. fu@mpip-mainz.mpg.de.
* Corresponding author: Fax +86-431-5262126; e-mail ychan@ciac.jl.cn.

10.1021/ma0483219 CCC: $30.25 © 2005 American Chemical Society
Published on Web 05/19/2005

at 155 °C and completely melt at 169 °C (T_{end}).[17] The Flory–Huggins interaction parameter (χ) between the PS and PLLA blocks can be estimated by $\chi(T) = 98.1/T - 0.112$ (T is the Kelvin temperature). Therefore, the copolymer studied here has strong repulsion at the experimental temperatures (χN(180 °C) = 24.0).[18] At T_g's < T < T_m, the copolymer can spontaneously segregate into the PLLA and PS lamellae. Besides, the PLLA blocks are able to crystallize. Therefore, this system permits the investigation of the interplay between crystallization and microphase separation.

2.2. Samples. Both homogeneous and heterogeneous PLLA-*b*-PS films were investigated. The homogeneous films were spin-coated from the solutions in the neutral solvent tetrahydrofuran (THF).[17] The film thickness was controlled by varying the solution concentration. To introduce nuclei into the films, a very small amount (less than 1% volume) of CS_2 (PS-selective) was added into the same THF solutions in order to induce the formation of tiny PLLA crystallites.[17] Freshly cleaned silicon ⟨100⟩ wafers with native oxide cover were used as the substrates. Before use, the silicon wafers were treated in a mixture of 70 mL of 98% sulfuric acid and 30 mL of 30% H_2O_2 solution at 80 °C for 20 min. After rinsing with deionized water for several times, the wafers were blown dry with compressed nitrogen gas. The spin-coated films were stored at 40 °C in a vacuum for at least 72 h in order to remove the residual solvent which may lead to the formation of fractal patterns in thin films.[19] The film thickness can be measured by X-ray reflectometry (Bruker, D8 XRR at 40 kV, 40 mA) or by scanning the edge of a scratched area with the atomic force microscope (AFM). Both methods provided identical thickness values within experimental error.

2.3. In Situ Atomic Force Microscopy (AFM). For in situ investigation of the copolymer thin films, a commercial scanning probe microscope (SPA300HV/SPI3800N, Seiko Instruments, Japan) was operated in tapping mode in a vacuum (10^{-5}–10^{-7} Torr), using a silicon cantilever (nominal spring constant ~2 N/m and resonant frequency ~70 kHz) with integrated conical tip (radius of curvature of ~20 nm). A hot stage supported on a 150 μm piezo tube scanner was used to heat the samples mounted on the stage. The sample temperature was monitored by a pair of thermocouple that was calibrated using standard gallium, indium, and tin samples before use. The temperature accuracy is ±1 °C. The samples were heated from room temperature with a rate no faster than 3 °C/min to the desired temperatures. Immediately, the tip was engaged to the sample surface by driving the piezo tube to raise the sample up and then the scan started. Thus, the scan may have several seconds delay after the engaging. The morphology evolution was recorded by continuous AFM scan, with both topography (height) and phase images.

During the scanning, it is not necessary to heat the cantilever since the influence of the thermal flux is negligible for the thin films in the vacuum chamber.[20]

2.4. X-ray Photoelectron Spectroscopy (XPS). XPS spectra of the PLLA-*b*-PS films before and after annealing at 180 °C were obtained with VG ESCALAB MKII (VG Co., UK) at room temperature by using an Mg Kα X-ray source ($h\nu$ = 1253.6 eV) at 14 kV and 20 mA. The instrument was kept in a vacuum chamber with a pressure of 10^{-7} Pa. The takeoff angle is 90°, corresponding to a detection depth less than 10 nm to the surface.

3. Results and Discussion

3.1. Equilibrium Morphology. Generally in molten thin films at $T < T_{ODT}$, if the blocks have preferential wettability to the substrate and the free surface (polymer/air interface), the copolymer chains can be oriented along the normal of the film/substrate interface, leading to lamellar structure parallel to the surface and interface.[21–23] Such orientation is usually determined by the competition between the polymer–substrate affinity, the surface tensions of the polymers, and the entropy penalty involved in the adjustment of the chain conformation. The entropy penalty may be dominant as the polymer molecular weight is very large, and the difference of surface tensions of the blocks is quite low (but not zero).[24] In this work, since the molecular weight is not very high, we assume that the enthalpy contributions (i.e., the polymer–substrate and polymer–surface interactions) determine the orientation of the copolymer chains as annealed above T_m^{PLLA}. The surface tension (fold surface energy from melt) of PLLA[25] is 60.89 mN/m, and that of PS[26] is 39.4 mN/m (at 20 °C). Therefore, the PLLA blocks wet the polar SiO_x surface and the PS blocks wet the free surface to minimize the surface energy, composing an asymmetric boundary condition. This scheme is examined by rapidly heating the spin-coated PLLA-*b*-PS films to the temperatures well above the T_m^{PLLA}. For example, the films quenched from the melt at 170–180 °C to room temperature show the typical morphologies which are determined by the quantization of film thickness by the lamellar spacing (L_0 = 20 nm[27]), as summarized in Figure 1. The films having thickness of $(m + {}^1/_2)L_0$ (m = 0, 1, 2, 3, ...) remained stable during annealing (for example, m = 0 in Figure 1a, the film was scratched in order to measure the film thickness with AFM; similar results were also obtained for films with thickness of 50, 90, and 110 nm). Otherwise, islands (Figure 1b), bicontinuous pattern (Figure 1c), and holes (Figure 1d) emerged on the free surface. Similar surface morphologies have been widely reported and reviewed.[21–23,28]

The segregation of PS blocks to the free surface was verified by measuring the XPS spectra and the water contact angles of the films before and after annealing (see Supporting Information). The C 1s peak at 289.0 eV corresponding to the carbonyl group indicates the existence of PLLA blocks at the surface of the spin-coated films. After annealing, this signal disappeared, and only the signal for the C–C bonds remained, indicating the segregation of PLLA blocks to the internal of the films and the PS to the surface. The segregation of the PS blocks to the surface is also verified by measuring the water contact angles (CAs) of the films before and after annealing at 180 °C: the CA values increased from ~80° before annealing to ~91° (which is closer to the CA value of PS) after annealing. Such segregation is valid for all the thin films investigated here (10–110 nm). Therefore, we conclude that the copolymer chains are perpendicularly oriented by the surface and substrate, forming lamellar structure parallel to the substrate.

Similar orientation has been widely reported for thin films of polystyrene-*block*-poly(methyl methacrylate) (PS-*b*-PMMA),[21–23] polystyrene-*block*-poly(4-vinylpyridine) (PS-*b*-P4VP),[29] and many other blocks with different polarity or surface tensions. For crystalline–coil diblocks (e.g., hydrogenated polybutadiene-*block*-poly(ethylene oxide), PB_h-*b*-PEO), such ordered lamellar structure will confine the crystallization because of the strong incompatibility between the blocks.[8–12] In this work, however, we are curious on the interplay between the crystallization and microphase separation as they are simultaneously possible. Therefore, instead of cooling the melt to below T_m^{PLLA}, the spin-coated films are heated to between the T_g^{PS} and T_m^{PLLA}. The results are presented below.

3.2. Homogeneous Thin Films: Spinodal Decomposition and Abnormal Relief Pattern. 3.2.1. Morphology Evolution. Homogeneous films of PLLA-*b*-

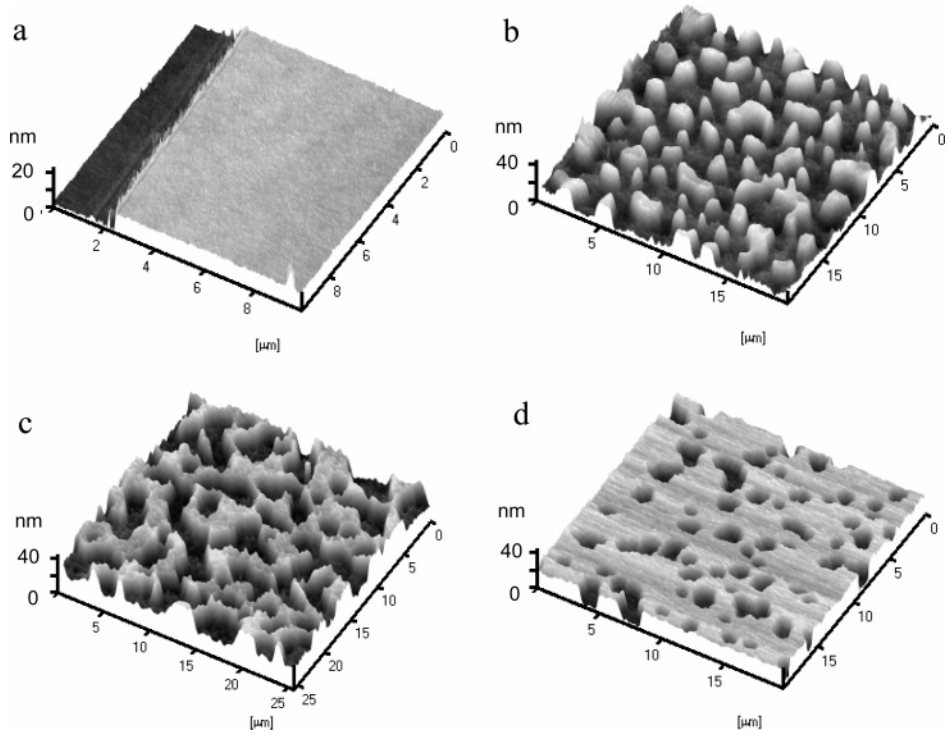

Figure 1. 3D view of the tapping mode AFM height images of the typical surface patterns of the PLLA-*b*-PS thin films quenched from melts at 175 °C: (a) 10 nm film with a scratch showing the film thickness with respect to the silicon wafer substrate; (b) 36, (c) 40, and (d) 27 nm.

PS can be obtained by spin-coating the dilute solutions in THF.[17] The films are amorphous and in disordered state since the neutral solvent has an effect of shielding the unfavorable contact of different blocks. Because of the strong incompatibility between the PLLA and PS blocks, however, such films are thermodynamically unstable and will undergo microphase separation as the temperature is well above T_g^{PS} and below the order−disorder transition temperature (T_{ODT}). In this work, such microphase separation process was investigated by in situ AFM in tapping mode with a hot stage. Figure 2 displays three typical successive surface morphologies at the early stage of two films with the thickness of 27 nm (Figure 2a−c) and 58 nm (Figure 2d−f). In both cases, the free surface began to fluctuate as the temperature increased above T_g^{PS}. Such fluctuation rapidly amplified into bicontinuous pattern. At this stage, the amplitude increased symmetrically toward the lamellar spacing of the symmetric PLLA-*b*-PS, according to the corresponding cross-section line scan profiles. Thus, the films were ordered; the free energy was reduced. This instability resembles the spinodal decomposition that was described in real space by Joly and co-workers.[30,31]

The spinodal-like pattern at the free surface can be characterized by the two-dimensional fast Fourier transform (2D FFT), which gives out the wavevector q of the surface pattern. Since the films are off-critical system, this decomposition is thermodynamically favorable; though, the kinetics is controlled by the mobility of the copolymer chains, which is a function of the temperature. For example, at 104 °C, the films began to fluctuate slowly, with the surface roughness advancing almost symmetric with respect to the average value (see the cross-section profile lines below Figure 2a,b). Such symmetric height distribution almost persists for a long time until the pattern height reaches the L_0 of PLLA-*b*-PS (Figure 2c and the profile line). As the temperature was elevated to 110 °C, the amplitude of the surface fluctuation rapidly reached L_0 (Figure 2d−f). At this stage, the copolymer chains are oriented by the surface and the substrate. Moreover, the polymer chains may be stretched since the blocks are strongly incompatible.

3.2.2. The Early Stage Kinetics. The early stage kinetics of the films is summarized in Figure 3. The 27 nm films underwent two kinetic regimes, with the crossover indicated by the arrows. At 104 °C, the q value almost remained constant at the earliest 65 min. This may indicate an extremely slow kinetics at the very early stage at this temperature although the reason is not clear yet. Afterward, q decayed with a power law of the annealing time (t), i.e., $q \propto t^n$. As the temperature was elevated to 110 and 125 °C, the molecular motion was activated. Thus, the very early stage crossover was not observed due to the limited time resolution of AFM. The surface q decayed as t^n, with the exponent n changing from about −1/3 to −0.63 at ∼233 min (110 °C) or at ∼24 min (125 °C). These crossover times correspond to the ordering of the chains; the surface pattern reached the typical height of L_0 (∼20 nm). That is, the copolymer chains are oriented along the substrate normal. The regime of the chain motions changed since the repulsion between the blocks was relaxed, and the line tension dominates. In this aspect, we define the stage before the crossover as the early stage and the one after the transition as the late stage. Thus, the early stage kinetics of the spinodal decomposition can be described by $q \propto t^n$, where $n \approx -1/3$ except at 104 °C.

3.2.3. Abnormal Relief Pattern. In this work, the lamellar spacing remained 20 nm for very long time at 110 °C. Only as the temperature is elevated to 125 °C was the lamellar spacing increased. Figure 4 displays the typical morphologies and the corresponding cross-section line scan profiles of the surface pattern of the 27 nm film at 125 °C.

Shortly after the amplitude of the spinodal like pattern rapidly increased to 20 nm (L_0) (Figure 4a), an

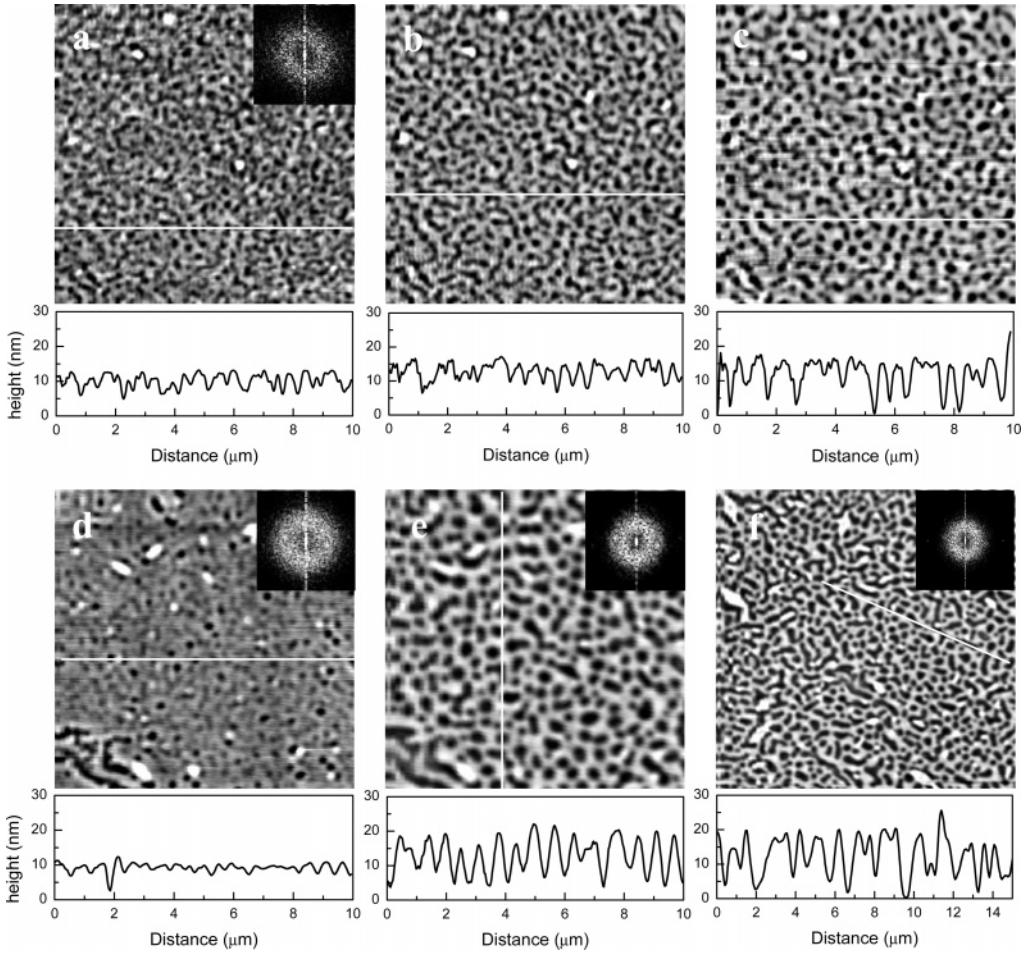

Figure 2. Surface morphology evolution (height images) of the homogeneous PLLA-*b*-PS films by in situ tapping mode AFM: (a−c) 27 nm film at 104 °C for (a) 35, (b) 76, and (c) 156 min; (d−f) 52 nm film at 107 °C for (d) 13, (e) 77, and (f) 207 min. The insets are the corresponding 2D FFT patterns.

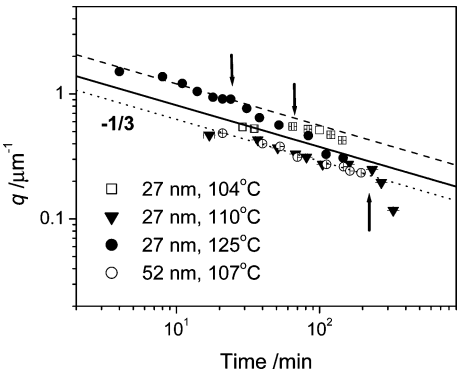

Figure 3. Kinetics of the spinodal-like pattern at the free surface of the homogeneous films. The error bars are smaller than the symbol.

abnormal "step" (as denoted as domain II in Figure 4b) started to grow on the original relief pattern (domain I in Figure 4b). From the corresponding cross-section profile, the abnormal pattern has a relative height of ∼8−12 nm (∼10 nm in average) with respect to the domain I. With the growth of domain II area (S_{II}), the total area of the surface pattern ($S_I + S_{II}$) decreased gradually, as shown in Figure 5a. The mass conservation requires

$$S_I(t_0)\bar{h}_I(t_0)\rho_I = S_I(t)\bar{h}_I(t)\rho_I + S_{II}(t)\bar{h}_{II}(t)\rho_{II}(t) \quad (1)$$

where $\bar{h}_i(t)$ is the average relative height of domain i with respect to the copolymer brush on the substrate at time t, t_0 denotes the starting time, and ρ_i is the density of domain i.

Similarly, many groups have reported the enhancement in lamellar spacing and film contraction in thin films of strongly incompatible crystalline−coil diblock copolymers.[11] The chain stretching during microphase separation was argued to favor chain folding, leading to an increase in the lamellar spacing.[13] In this study, the PLLA blocks may also crystallize when the incompatible PS and PLLA blocks strongly repulse and stretch each other. From Figure 5a, it is convenient to estimate that $S_I(t_0) \approx 570\ \mu m^2$, $S_I(t_{end}) \approx 130\ \mu m^2$, and $S_{II}(t_{end}) \approx 270\ \mu m^2$; assuming $\bar{h}_I(t_0) = \bar{h}_I(t) \approx 20$ nm and $\bar{h}_{II}(t) \approx 30$ nm, one immediately gets $\rho_{II} \approx 1.086\rho_I$. This increase in the density of domain II with respect to that of domain I may imply a highly compact condensation of the copolymer chains. For the PLLA chains, it is likely that the chains adopt folded conformation; namely, the PLLA block might crystallize (the density $\rho_{amorph} = 1.248$ g/cm^3, $\rho_{cryst} = 1.290$ g/cm^3).[25] However, the crystal structure cannot be confirmed by any characterization methods by far. This may have two reasons. First, the PLLA homopolymer usually has very low crystallinity (∼37%) in bulk.[25] Second, polymer crystallization in confined geometry could be highly frustrated due to the additional entropic penalty induced by the change of the chain conformation. Thus, it may be hard for the PLLA blocks to fold into perfect lattice. Recently, Ho and co-

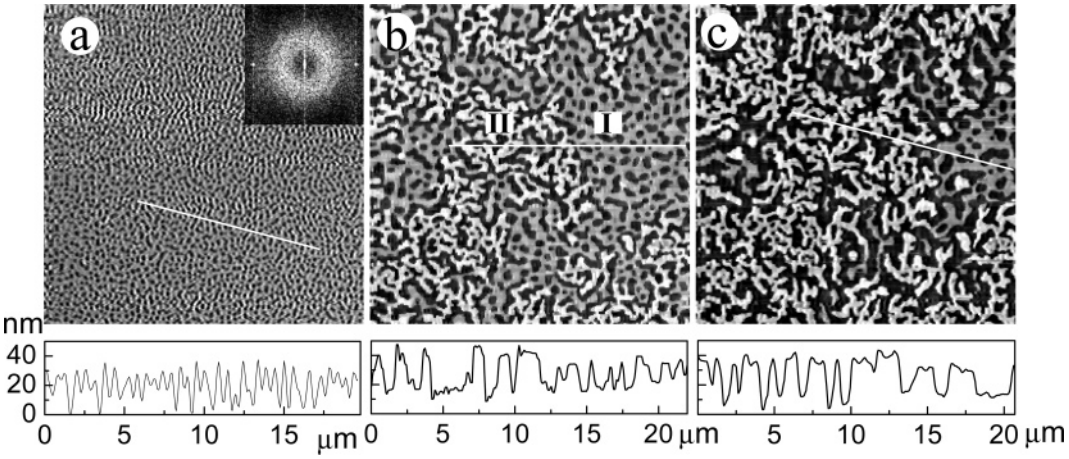

Figure 4. Nucleation and growth of the abnormal relief structure on the spinodal pattern of the 27 nm film at 125 °C by in situ tapping mode AFM (height images). (a) 3, (b) 107, and (c) 477 min. The corresponding cross-section line profiles show that domains I have a height of ~20 nm (L_0) and domains II have a height of ~30 nm, with respect to the sublayer.

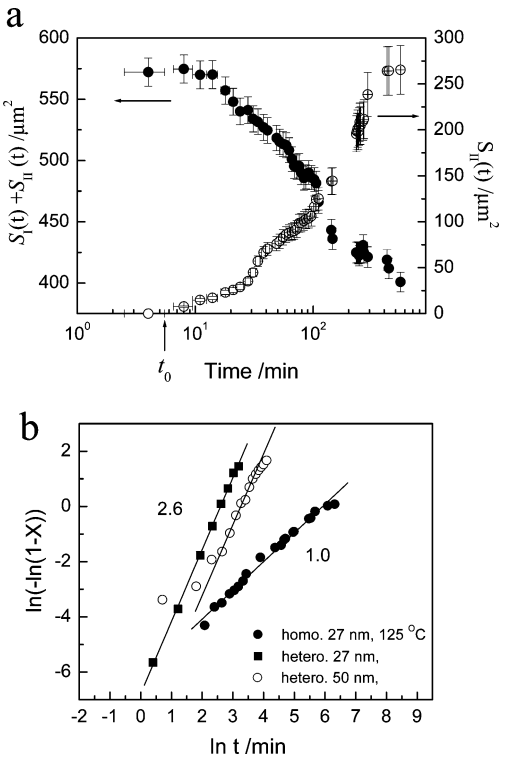

Figure 5. (a) Evolution of the total area of the surface relief pattern, $S_I + S_{II}$ (●), and the area of domains II, S_{II} (○), within the scan area. (b) The $\ln(-\ln(1 - X(t)))$ vs $\ln t$ plot of the thin films, where $X(t)$ is the transformation ratio of the surface pattern, as explained in the text.

workers[32] investigated the PLLA crystallization within the mesophase of the bulk PS−PLLA from ordered melt. Such confined crystallization was found to induce undulation of the PS−PLLA lamellae by a proposed stress-induced mechanism. In our case, no similar undulated morphology was found even the temperature was well above the T_g^{PS}. The confinement from the hard substrate and the impenetrable air/polymer interface may provide very strong constraint of the copolymer chains. Thus, it may be hard for the PLLA blocks to adopt favorable conformation to form perfect lattice.

For the convenience of describing the kinetics of the evolution of domains II, however, we approximately define the degree of transformation from domains I to domains II

$$X(t) = \frac{S_{II}(t)}{S_I(t_0)} \tag{2}$$

The $X(t)$ values are summarized in Figure 5b as solid circles; the growth kinetics of domains II can be described by the Avrami equation

$$\ln(1 - X) = -Kt^n \tag{3}$$

where t is the annealing time and the prefactor K and the exponent n are Avrami constants. The slope of the fitting line in Figure 6b yields $n = 1.0$. Although the exact crystallinity within domain II is not available, it may be reasonable to assume that the crystallinity is proportional to the area of domain II. Thus, to some extent, the Avrami kinetic may reflect the kinetics of the PLLA crystallization.

3.3. Heterogeneous Films with Self-Assembled Nuclei: Crystallization and Subsequent Nucleation of Holes. Previously, we succeeded in fabricating the (semi)crystalline assemblies by the addition of PS-selective solvent (e.g., CS_2) into the PLLA-*b*-PS/THF solutions.[17] In this work, a very small content of CS_2 (less than 1 wt %) was slowly added into the THF solutions in order to create semicrystalline nuclei in the spin-coated thin films, as seen in Figure 6a. Two kinds of typical orientations of the nuclei, i.e., flat-on (Figure 6b,c) and edge-on (Figure 6d,e), are found on the film surface according to the AFM height and phase images. Previously, it was demonstrated that such semicrystalline structures are open to the films.[17,27] At temperatures between the T_g^{PS} and T_m^{PLLA}, the PLLA began to crystallize. The snapshots in Figure 8 show the crystallization of the 27 nm copolymer films with nuclei. Dendritic pattern started at the nuclei and expanded anisotropically (Figure 7b). No apparent difference in the behaviors of the flat-on and edge-on nuclei was found. The dendritic crystallites grew laterally, encountered each other (Figure 7c), and finally covered the whole surface of the film (Figure 7d). No spherulites were observed on the surface. With long time annealing, or at elevated temperatures (e.g., 137 °C), further crystallization resulted in many cracks in the films (Figure 7e). In thicker films, on the other hand, the copolymers usually crystallized into spherulites. For

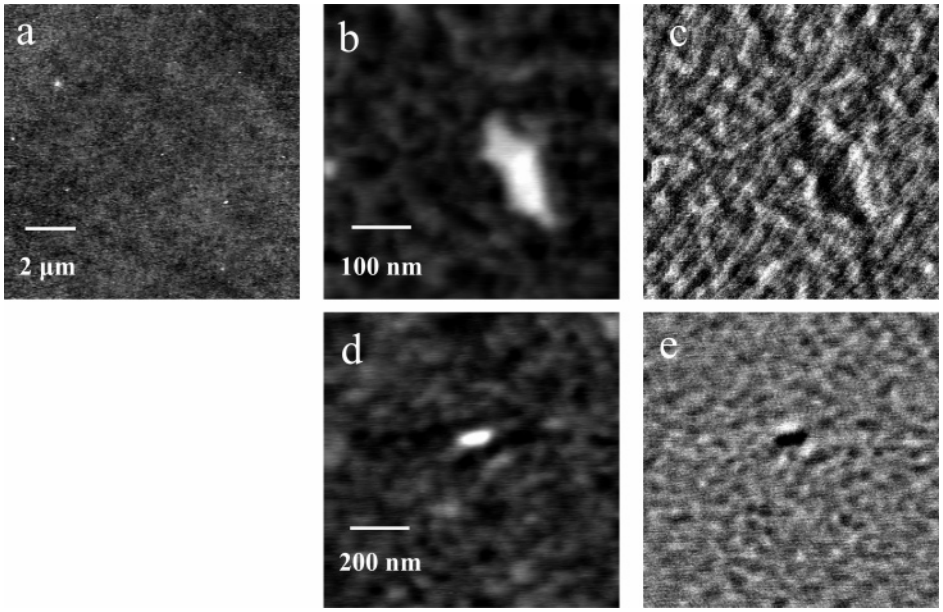

Figure 6. (a) Tapping mode AFM height image of the heterogeneous surface of the films spin-coated from PLLA-*b*-PS solutions in THF/CS_2 mixtures. The flat-on (b, c) and edge-on (d, e) nuclei are observed on the surface with tapping mode AFM height (b, d) and phase (c, e) images.

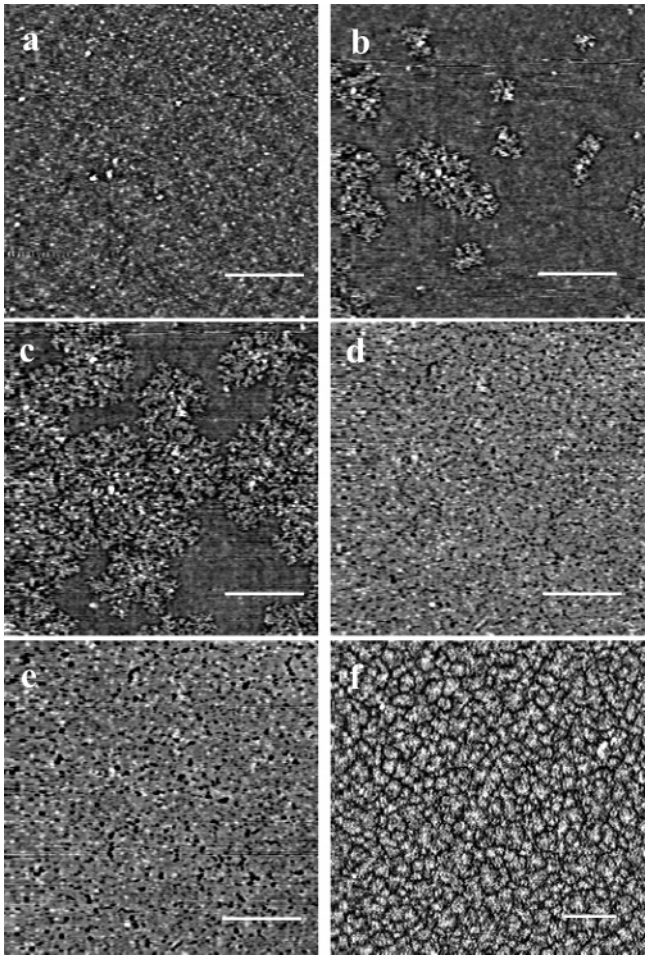

Figure 7. (a–d) In situ tapping mode AFM observation of the crystallization of the heterogeneous 27 nm film at 107 °C. (e) Further crystallization at 137 °C cracks the film. (f) The spherulites of the heterogeneous 110 nm film crystallized at 120 °C. All the images are AFM height images with the scales bars representing 10 μm.

example, as the 110 nm PLLA-*b*-PS films with nuclei were annealed at 120 °C, the PLLA rapidly crystallized, forming densely arranged spherulites in the films (Figure 7f). As the number density of the nuclei was reduced, spherulites of tens of micrometers in diameter could be obtained.

The specimen thickness dependence of the polymer crystallization was analyzed by Schultz,[33] considering the homogeneous nucleation from the melted films. The ratio of the film thickness to the growth velocity was found to determine the crystallization kinetics: thin films usually exhibit abnormal low Avrami exponent. The crystallization of PLLA in bulk and thin films has been widely investigated.[32,34,35] Ho and co-workers[32] compared the Avrami exponents (n) of the homopolymer PLLA and of the PLLA in the oriented PLLA-*b*-PS lamellae. With increasing crystallization temperatures from 70 to 120 °C, the n value could increase from 1.3 to 2.7.[32] This increase in n value as the temperature approached to T_g^{PS} was argued to indicate a significant transition from homogeneous ($n \approx 1$) to heterogeneous nucleation ($n > 1$). Very recently, the investigation of the cold crystallization of PLLA thin films by the infrared and two-dimensional correlation spectroscopy revealed crystallization kinetics with $n \approx 2$ at 78 °C.[34] This indicates the heterogeneous nucleation of the PLLA cold crystallization in thin films (thickness < 100 nm).

In our work, the kinetics of the films with nuclei are summarized in Figure 5b. The apparent crystallization degree ($X(t)$) was roughly defined as the ratio of the area of the dendrites to the area of the scanned image. This may be reasonable, assuming that the real crystallization degree of the PLLA in the dendrites (although not available yet) is the same all over the area. Thus, the slope of the fitting lines in the $\ln(-\ln(1 - X(t))$ vs $\ln t$ plot yields the n values of 2.6. For the heterogeneous films with different film thickness ($\leq$100 nm), this study always found the crystallization kinetics with $n > 1$. Occasionally, the Avrami exponent will be smaller for thicker films than that for the thinner ones. This apparent discrepancy to Schultz's theory[33] may root from the underestimation of the crystallization degree since, in thick films, the crystallites grow not only along the surface but also along the other directions. This

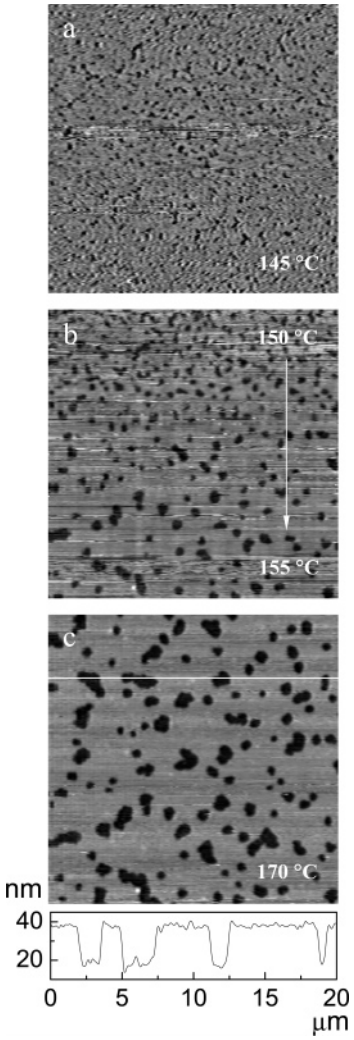

Figure 8. Tapping mode AFM height images show (a) the significant film cracking at 145 °C, (b) the melting of the crystallites and the nucleation of holes at the film surface with the temperature increasing from 150 to 155 °C within the scan time (~3 min), and (c) the coalescence and growth of the holes at 170 °C. The attaching cross section profile indicates the typical hole depth of ~20 nm (L_0).

latter contribution to the crystallization kinetics cannot be estimated by AFM observation. Therefore, systematic work is needed to examine the effect of the film thickness on the crystallization kinetics of block copolymers.

During the heterogeneous nucleation and crystallization process, no typical microphase separation pattern (spinodal-like or holes, islands) was observed. In this case, it is likely that the existence of the nuclei largely depressed the activation energy of crystallization for the PLLA blocks. Therefore, crystallization started once the temperature was well above the T_g^{PLLA}. The folding and incorporation of the PLLA chains into crystallites will be accompanied by the microphase separation[36] since the incompatible PS blocks cannot enter the PLLA lattice (although the lattice is highly imperfect). In this viewpoint, it is believable that the instability due to the incompatibility of the PS and PLLA blocks is largely relaxed.

At elevated temperatures, the films were cracked since the PLLA crystallites became more perfect (Figure 8a). For the 27 nm film, for example, such cracks nucleated the holes in the films as the temperature was

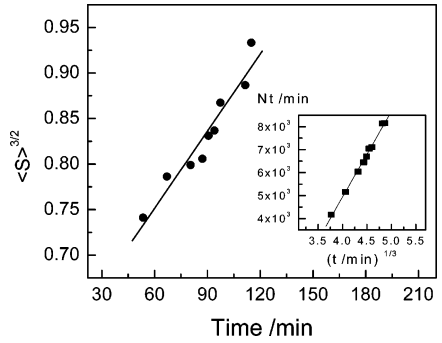

Figure 9. Coarsening kinetics of the holes at the surface of the heterogeneous 27 nm film at 170 °C.

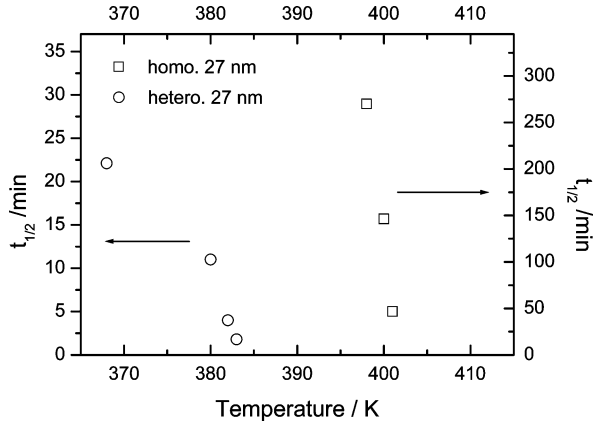

Figure 10. Comparison of the crystallization temperature dependence of the crystallization halftime ($t_{1/2}$) of the homogeneous (□) and heterogeneous (○) 27 nm films.

increased to 155 °C (T_m^{PLLA}) when the PLLA crystallites began to melt. The melting and nucleation process was displayed in Figure 8. This hole nucleation process is much different from the mechanism based on the local dislocation[37] and/or wrong lamellae[38] in the preordered films. At the early stage, the holes coalesced rapidly after nucleation, with the hole depth remaining ~20 nm (L_0). This indicates the establishment of the lamellar structure parallel to the substrate. As the films thickness was varied, islands or stable films were obtained at $T \gg T_m^{PLLA}$, depending on the quantization of the film thickness by the lamellar period (L_0).

At 170 °C, for example, the holes coarsened. Usually, Ostward ripening of holes (islands) is widely accepted for the coarsening kinetics, featured by 2/3 power law increase in the average area ($\langle S \rangle$) of holes (islands) with respect to the annealing time or −2/3 power law decay in the hole (island) number (N) with annealing time.[39] That is, $\langle S \rangle \sim t^{2/3}$ and $N \sim t^{-2/3}$, or $\langle S \rangle^{3/2} \sim t$ and $Nt \sim t^{1/3}$.[39] Using these scalings, the kinetics of the hole coarsening can be nicely described, as shown in Figure 9. The hole depth remained 20 nm during coarsening.

Remarkably, such microphase separation and crystallization from frozen disordered thin films are much different from those from disordered melt.[8] For crystallization from overcooled melts, the crystallization rate is primarily determined by the degree of overcooling. Therefore, the crystallization halftime ($t_{1/2}$) increases with increasing temperature (decreasing degree of overcooling). For the crystallization in the previously vitrified polymers, the copolymer chains could not relax or fold until the temperature increased above T_g. Figure 10 compares the temperature dependence of the $t_{1/2}$ of crystallization nucleated homogeneously and heteroge-

neously. The halftimes of both samples decrease with increasing temperature. Ho et al. reported that the crystallization halftimes of PLLA in bulk PLLA-*b*-PS mesophase decreased with increasing T_c at $T_c < 90$ °C and increased with increasing T_c at $T_c > 90$ °C, which was very similar to the behavior of bulk PLLA homopolymer (Figure 12 in ref 32). The confinement of the copolymers induced some retardation of the crystallization from melt so that the halftimes of PLLA-*b*-PS were increased with respect to those of homoPLLA.[32]

In Figure 10, it is remarkable that the halftimes are much longer than those reported by Ho et al., but rather closer to those reported by Zhang and co-workers, who examined the cold crystallization of PLLA thin films.[34] In Ho's case, the crystallization from melt is a nucleation-and-folding-controlled process since the polymer chains have already been activated; in our work, as well as in Zhang's case, the cold crystallization from vitrified films seems a relaxation-controlled process since it is necessary for the polymer chains to be sufficiently activated before they start to nucleate and fold. Normally, the polymer relaxation time (τ) at T_g is at the order of 100 s.[40] At higher temperatures, τ rapidly decreases. This is qualitatively consistent with the temperature dependence of the $t_{1/2}$ in Figure 10. Thus, it may be believable that the cold crystallization of PLLA-*b*-PS films is a relaxation-controlled process. However, because of the limitation of the low time resolution of in situ AFM, we are not able to investigate the temperature dependence of $t_{1/2}$ at $T \gg T_g^{PS}$. Remarkably, the $t_{1/2}$'s for the homogeneous 27 nm film are an order of magnitude larger than those for the heterogeneous ones. This may reflect the retardation induced by the confinement of the mesophases.

The homopolymer crystallization in thin films has recently been widely investigated by in situ AFM and spectroscopic methods.[20,34,41−46] The orientation of the polymer chains and the crystals largely depend on the film thickness and the nature of the substrates. In thick films (e.g., 2.5 μm), the crystals adopt the edge-on conformation, while in thin films (∼200 nm or lower), the flat-on crystals are prevailing.[44,45] Although the hot stage AFM permits the real-space investigation of the crystallization behavior from lamella to lamella and leads to many new findings complementary to our previous knowledge on polymer crystallization,[41−43] the overall crystallization kinetics by spectroscopic methods, for example, usually follows the classical laws.[34,44,45] In ultrathin films of poly(ethylene oxide) (PEO), Schönherr et al. observed the growth of the flat-on lamellae with in situ AFM and concluded that the crystallization of PEO in thin and ultrathin films is governed by the same laws as the bulk crystallization. This conclusion was also confirmed by their Fourier transform infrared (FT-IR) spectroscopy analysis that yielded crystallization kinetics with the Avrami exponents of 3.6−4.0. Similarly using IR, Zhang et al. reported the cold crystallization kinetics of PLLA in thin films with the Avrami exponent of ∼2.0.

In our case of the heterogeneous PLLA-*b*-PS thin films, however, no apparent orientation of the copolymer chains and the crystals was observed at the early stage. Only dendritic pattern for thin films (e.g., 27 nm) and spherulites for thicker films (e.g., 110 nm) were found. Within these patterns, no discernible lamellae have formed. This implies that the cold crystallization of the crystalline-coil PLLA-*b*-PS from the amorphous state may be different from the homopolymers. The linkage of the amorphous PS blocks may severely interrupt the folding of the PLLA blocks into perfect lattice because of the strong incompatibility between PS and PLLA. In very thin films, the formation of spherulites was prohibited, possibly due to the limited geometry of the films. In thicker films, very small spherulites (with several microns of diameter) were observed. Even though, no typical lamellae were found within such spherulites (Figure 8f and magnified images, not shown).

In microphase-separated lamellae, Zhu et al.[47] and Ho et al.[32] have investigated the orientation of the folded chains and the crystal stems. Zhu and co-workers found that the stem orientation of the PEO crystals depended on the crystallization temperature (T_c): the higher T_c could induce the orientation of the *c*-axis along the normal of the lamellar interface. The wide-angle X-ray diffraction (WAXD) data of Ho et al. also indicated that the PLLA chains also folded along the lamellar interface with the chain orientation perpendicular the interface of PLLA-*b*-PS lamellae in bulk.[32]

With respect to the abundant results on the chain orientation in bulk block copolymers,[5,32,47−50] less knowledge is known about the chain orientation in the thin films of block copolymers.[11,51,52] This may have several reasons. (1) In thin films on the substrates, it is likely that the strong interaction between the polymers and the substrate may largely depress the mobility of the chains.[53] The copolymer brush could be tightly anchored to the surface, which may in turn depress the mobility of the next above layer. (2) In thin films, the strong confinement of the impenetrable hard walls could constraint the mobility of the chains. The formation of perfect crystal lattice structure may cause large entropy penalty due to the substantial adjustment of the conformation of both PLLA and PS blocks. Therefore, at most, the PLLA chains may form very small crystallites at some local domains, with a large amount of amorphous PLLA phase surrounding them. By far, however, no signal indicating the crystallization of the PLLA in the PLLA-*b*-PS thin films is available.

Previously, the first-order crystallization has ever been reported for polymers under high rate stretching, where the orientation of the polymer chains was argued to induce massive nucleation.[54] Recently, quiescent first-order crystallization of polyethylene blocks confined in meosphases has been reported and argued as homogeneous nucleation.[8,11] In the nanoconfined geometry, the chain crystallization is likely to accomplish instantaneously upon nucleation. In the PLLA lamellae of our work, the proposed crystallization of each PLLA chain can be accomplished very fast since the available space is less than 5 nm ((L_0/2)/2), which is less than the *c*-axis length (10_3 helix) of a unit cell in bulk.[55] Thus, the crystallization of a single chain could be finished once it was nucleated.[8,11,15] Therefore, the crystallization kinetics depends on the polymers yet to be nucleated. In the case of homogeneous films, such nucleation could be induced by the highly stretched copolymer chains due to the strong incompatibility of the diblocks.[8,15,27]

4. Conclusion

The early stage interplay of the crystallization and microphase separation is investigated by comparing the early stage evolution of the homogeneous and heterogeneous thin films of PLLA-*b*-PS diblocks at temperatures between T_g and T_m. The diblocks in homogeneous

films segregated through spinodal decomposition and such vertical ordering and stretching of the blocks initiated the PLLA crystallization which increased the lamellar spacing by a factor of 50%. Using a tiny amount of CS_2, semicrystalline nuclei were successfully integrated into the thin films without significantly changing the film thickness. Thus, the behavior of the heterogeneous PLLA-*b*-PS films can be compared with that of the homogeneous ones. At $T > T_g^{PS}$, dendritic crystals were obtained for thin films (e.g., 27, 50 nm), while spherulites were observed in thicker films (e.g., 86, 110 nm). The thermodynamic instability of the unlike diblock copolymer chains was relaxed by the chain folding of PLLA blocks and the exclusion of the PS from the PLLA domains, although the well-ordered mesophase was not formed. As a result, no classical spindoal-like or islands/holes structures were observed until the films were annealed at $T \geq T_m^{PLLA}$. At high temperatures, the crystals melted and the films decomposed at the cracks induced by the crystallization prior to the melting.

Using in situ AFM with a hot stage, we are able to investigate the kinetics of the microphase separation, crystallization, and the interplay of both processes. The homogeneous films decomposed in a spinodal-like manner, with the surface wavevector q decayed as $t^{-1/3}$. The growth of the abnormal relief pattern (domain II) can be nicely described by the first-order Avrami equation, which, together with the fact that this pattern had a high density and melted at T_m^{PLLA}, might indicate that the PLLA blocks crystallized within domain II. On the other hand, the integration of nuclei induced remarkable change of the molecular motions of the copolymer chains. Crystallization with the Avrami exponent of ~2.6 dominated, which indicates a heterogeneous nucleation and multidimensional growth of the crystals (although very imperfect).

We also compared the PLLA crystallization halftimes ($t_{1/2}$'s) of the homogeneous and heterogeneous films as well as with the reported $t_{1/2}$'s of PLLA in bulk PLLA-*b*-PS. Our values are much larger than those in bulk. Moreover, the $t_{1/2}$'s decreased with the increasing of the crystallization temperature within the temperature range considered here. These factors may have an implication that the cold crystallization of the PLLA blocks is a relaxation-controlled process.

However, because of the low crystallinity of PLLA and the involvement of amorphous PS blocks, it is by far hard to directly resolve the crystallization structure within these thin films. The actual crystallization kinetics is still not accessible yet. The topic on the interplay of the crystallization and microphase separation may be extended by, for example, using very fast AFM[41,42] and the combination of many other advanced techniques.[56]

Acknowledgment. The authors are indebted to the financial support from the National Natural Science Foundation of China (50125311, 20334010, 20274050, 50390090, 50373041, 20490220, 20474065, 50403007), the Ministry of Science and Technology of China (2003CB615601), the Chinese Academy of Sciences (Distinguished Talents Program, KJCX2-SW-H07), and the Jilin Distinguished Young Scholars Program (20010101).

Supporting Information Available: Contact angles and XPS spectra of the PLLA-*b*-PS thin films before and after annealing as well as that of the PLLA homopolymer. This material is available free of charge via the Internet at http://pubs.acs.org.

References and Notes

(1) Bates, F. S.; Fredrickson, G. H. *Annu. Rev. Phys. Chem.* **1990**, *41*, 525.
(2) Hamley, I. W. *The Physics of Block Copolymers* Oxford University Press: Oxford, 1998.
(3) Dalvi, M. C.; Lodge, T. P. *Macromolecules* **1994**, *27*, 3487.
(4) Hamley, I. W. *Adv. Polym. Sci.* **1999**, *148*, 113.
(5) Mai, S.-M.; Fairclough, J. P. A.; Viras, K.; Gorry, P. A.; Hamley, I. W.; Ryan, A. J.; Booth, C. *Macromolecules* **1997**, *30*, 8392.
(6) Qurim, D. J.; Register, R. A.; Marchand, G. R.; Adamson, D. H. *Macromolecules* **1998**, *31*, 4891.
(7) Li, L.; Séréro, Y.; Koch, M. H. J.; de Jeu, W. H. *Macromolecules* **2003**, *36*, 529.
(8) Loo, Y.-L.; Register, R. A.; Ryan, A. J. *Phys. Rev. Lett.* **2000**, *84*, 4120.
(9) Loo, Y.-L.; Register, R. A.; Ryan, A. J. *Macromolecules* **2002**, *35*, 2365.
(10) Lee, W.; Chen, H.-L.; Lin, T.-L. *J. Polym. Sci., Part B: Polym. Phys.* **2002**, *40*, 519.
(11) Optiz, R.; Lambreva, D. M.; de Jeu, W. H. *Macromolecules* **2002**, *35*, 6930.
(12) Reiter, G.; Castelein, G.; Sommer, J.-U.; Röttele, A.; Thurn-Albrecht, T. *Phys. Rev. Lett.* **2001**, *87*, 226101.
(13) Reiter, G.; Castelein, G.; Hoerner, P.; Riess, G.; Sommer, J.-U.; Floudas, G. *Eur. Phys. J. E* **2000**, *2*, 319.
(14) Mayes, A. M.; Russell, T. P.; Bassereau, P.; Baker, S. M.; Smith, G. S. *Macromolecules* **1994**, *27*, 749.
(15) Zhang, F.; Chen, Y.; Huang, H.; Hu, Z.; He, T. *Langmuir* **2003**, *19*, 5563.
(16) Tao, L.; Luan, B.; Pan, C. Y. *Polymer* **2003**, *44*, 1013.
(17) Fu, J.; Luan, B.; Yu, X.; Cong, Y.; Li, J.; Pan, C.; Han, Y.; Yang, Y.; Li, B. *Macromolecules* **2004**, *37*, 976.
(18) Zalusky, A. S.; Olayo-Valles, R.; Wolf, J. H.; Hillmyer, M. A. *J. Am. Chem. Soc.* **2002**, *124*, 12761.
(19) Lee, S.-H.; Kang, H.; Kim, Y. S.; Char, K. *Macromolecules* **2003**, *36*, 4907.
(20) Schönherr, H.; Bailey, L. E.; Frank, C. W. *Langmuir* **2002**, *18*, 490.
(21) Coulon, G.; Russell, T. P.; Deline, V. R.; Green, P. F. *Macromolecules* **1989**, *22*, 2581.
(22) Russell, T. P.; Coulon, G.; Deline, V. R.; Miller, D. C. *Macromolecules* **1989**, *22*, 4600.
(23) Mansky, P.; Russell, T. P. *Macromolecules* **1995**, *28*, 8092.
(24) (a) Busch, P.; Posselt, D.; Smilgies, D.-M.; Rheinländer, B.; Kremer, F.; Papadakis, C. M. *Macromolecules* **2003**, *36*, 8717. (b) Potemkin, I. I. *Macromolecules* **2004**, *37*, 3505.
(25) Mark, J. E. *Polymer Data Handbook*; Oxford University Press: New York, 1999.
(26) Brandrup, J., Immergut, E. H., Grulke, E. A., Abe, A., Bloch, D. R., Eds.; *Polymer Handbook*, 4th ed.; John-Wiley & Sons: New York, 1999.
(27) Fu, J.; Cong, Y.; Li, J.; Luan, B.; Pan, C.; Yang, Y.; Li, B.; Han, Y. *Macromolecules* **2004**, *37*, 6918.
(28) Green, P. F.; Limary, R. *Adv. Colloid Interface Sci.* **2001**, *94*, 53.
(29) Peters, R. D.; Yang, X. M.; Kim, T. K.; Sohn, B. H.; Nealey, P. F. *Langmuir* **2000**, *16*, 4625.
(30) Joly, S.; Raquois, A.; Paris, F.; Hamdoun, B.; Auvray, L.; Ausserre, D.; Gallot, Y. *Phys. Rev. Lett.* **1996**, *77*, 4394.
(31) This spinodal decomposition is different from the spinodal dewetting of the diblock copolymers at the temperatures above their T_{ODT}. See, for example: Renger, C.; Müller-Buschbaum, P.; Stamm, M.; Hinrichsen, G. *Macromolecules* **2000**, *33*, 8388−8398. Müller-Buschbaum, P.; Gutmann, J. S.; Lorenz-Haas, C.; Wunnicke, O.; Stamm, M.; Petry, W. *Macromolecules* **2002**, *35*, 2017. Limary, R.; Green, P. F. *Langmuir* **1999**, *15*, 5617; *Macromolecules* **1999**, *32*, 8167; *Macromolecules* **2002**, *35*, 6486.
(32) Ho, R.-M.; Lin, F.-H.; Tsai, C.-C.; Lin, C.-C.; Ko, B.-T.; Hsiao, B. S.; Sics, I. *Macromolecules* **2004**, *37*, 5985.
(33) Schultz, J. M. *Macromolecules* **1996**, *29*, 3022.
(34) Zhang, J. M.; Tsuji, H.; Noda, I.; Ozaki, Y. *Macromolecules* **2004**, *37*, 6433.
(35) Vasanthakumari, R.; Pennings, A. J. *Polymer* **1983**, *24*, 175.
(36) Quiram, D. J.; Register, R. A.; Marchand, G. R. *Macromolecules* **1997**, *30*, 4551.

(37) Grim, P. C. M.; Nyrkova, I. A.; Semenov, A. N.; ten Brinke, G.; Hadziioannou, G. *Macromolecules* **1995**, *28*, 7501.
(38) Joly, S.; Ausserré**,** D.; Brontons, G.; Gallot, Y. *Eur. Phys. J. E* **2002**, *8*, 355.
(39) (a) Bassereau, P.; Brodbreck, D.; Russell, T. P.; Brown, H. R.; Shull, K. R. *Phys. Rev. Lett.* **1993**, *71*, 1716. (b) Ardell, A. J. *Phys. Rev. Lett.* **1995**, *74*, 4960.
(40) McCrum, N. G.; Read, B. E.; Williams, G. *Anelastic and Dielectric Effects in Polymeric Solids*; Wiley: London, 1967.
(41) Hobbs, J.; Miles, M. J. *Macromolecules* **2001**, *34*, 353.
(42) Hobbs, J.; Humphris, A. D. L.; Miles, M. J. *Macromolecules* **2001**, *34*, 5508.
(43) Beekmans, L. G. M.; Valée, R.; Vancso, G. J. *Macromolecules* **2002**, *35*, 9383.
(44) Schönherr, H.; Frank, C. W. *Macromolecules* **2003**, *36*, 1188.
(45) Schönherr, H.; Frank, C. W. *Macromolecules* **2003**, *36*, 1199.
(46) Schönherr, H.; Waymouth, R. M.; Frank, C. W. *Macromolecules* **2003**, *36*, 2412.
(47) Zhu, L.; Cheng, S. Z. D.; Calhoun, B. H.; Ge, Q.; Quirk, R. P.; Thomas, E. L.; Hsiao, B. S.; Yeh, F.; Lotz, B. *J. Am. Chem. Soc.* **2000**, *122*, 5957.
(48) Hamley, I. W.; Fairclough, J. P. A.; Terrill, N. J.; Ryan, A. J.; Lipic, P. M.; Bates, F. S.; Towns-Andrews, E. *Macromolecules* **1996**, *29*, 8835.
(49) Douzinas, K.; Cohen, R. E. *Macromolecules* **1992**, *25*, 5030.
(50) Ryan, A. J.; Fairclough, J. P. A.; Hamley, I. W.; Mai, S.-M.; Booth, C. *Macromolecules* **1997**, *30*, 1723.
(51) Hong, S.; MacKnight, W. J.; Russell, T. P.; Gido, S. P. *Macromolecules* **2001**, *34*, 2398.
(52) Hong, S.; MacKnight, W. J.; Russell, T. P.; Gido, S. P. *Macromolecules* **2001**, *34*, 2876.
(53) van Zanten, J. H.; Wallace, W. E.; Wu, W. *Phys. Rev. E* **1996**, *53*, R2053.
(54) Kalb, B.; Pennings, A. J. *Polymer* **1980**, *21*, 607.
(55) Blundell, D. J.; MacKerron, D. H.; Fuller, W.; Mahendrasingam, A.; Martin, C.; Oldman, R. J.; Rule, R. J.; Riekel, C. *Polymer* **1996**, *37*, 1330.
(56) Organ, S. J.; Hobbs, J. K.; Miles, M. J. *Macromolecules* **2004**, *37*, 4562.

MA0483219